RESEARCH ARTICLE | AUGUST 27 2026

Stacking-engineered thermal transport and phonon filtering in rhenium disulfide

Yongjian Zhou ; Haoran Cui ; Zefang Ye; Jung-Fu Lin ; Yan Wang ; Yaguo Wang

Appl. Phys. Lett. 129, 082107 (2026)
https://doi.org/10.1063/5.0342816

Applied Physics Letters ARTICLE pubs.aip.org/aip/apl

Stacking-engineered thermal transport and phonon filtering in rhenium disulfide

Cite as: Appl. Phys. Lett. **129**, 082107 (2026); doi: 10.1063/5.0342816
Submitted: 8 May 2026 · Accepted: 3 August 2026 ·
Published Online: 27 August 2026

View Online Export Citation CrossMark

Yongjian Zhou,[1] Haoran Cui,[2] Zefang Ye,[1] Jung-Fu Lin,[3] Yan Wang,[2,a)] and Yaguo Wang[1,a)]

AFFILIATIONS

[1]Walker Department of Mechanical Engineering, The University of Texas at Austin, Austin, Texas 78712, USA
[2]Department of Mechanical Engineering, University of Nevada, Reno, Reno, Nevada 89557, USA
[3]Department of Geological Sciences, Jackson School of Geosciences, The University of Texas at Austin, 2305 Speedway Stop C1160, Austin, Texas 78712, USA

[a)]**Authors to whom correspondence should be addressed:** yanwang@unr.edu and yaguo.wang@austin.utexas.edu

ABSTRACT

Cross-plane heat transport is a critical bottleneck for van der Waals (vdW) electronics, yet its microscopic governing principles remain elusive. We demonstrate that stacking order is an effective control knob for cross-plane phonon transport in multilayer rhenium disulfide (ReS_2). Thickness-dependent thermal conductivity measurements reveal remarkably long cross-plane phonon mean free paths ($\gtrsim$200–300 nm) and provide a direct experimental observation of the transition from quasi-ballistic transport to a ballistic regime characterized by thickness-independent thermal resistance. AA stacking exhibits nearly double the cross-plane thermal conductivity of AB stacking, driven by longer acoustic phonon lifetimes associated with the more closely aligned interlayer registry of AA stacking. Deep-neural-network-based molecular dynamics simulations reveal that phonon filtering in ReS_2 is fundamentally frequency-selective: weak vdW coupling acts as a low-pass filter, whereas stronger coupling broadens the transmission passband. These results establish ReS_2 as a model system where stacking order and interlayer coupling can be engineered to tune heat conduction across diffusive, quasi-ballistic, and ballistic regimes, offering a new framework for thermal management in two-dimensional electronics.

ReS_2 has emerged as a versatile two-dimensional (2D) material that is widely investigated for photodetectors, ultrafast saturable absorbers, and other optoelectronic applications owing to its high photoresponsivity, broadband absorption, and strong nonlinear optical response.[1–3] ReS_2 crystallizes in a distorted 1T triclinic structure in which rhenium atoms form zigzag chains. This low-symmetry lattice dramatically enhances in-plane anisotropy and, when combined with weak interlayer van der Waals (vdW) coupling, endows ReS_2 with physical properties that are highly sensitive to structural registry. Multilayer ReS_2 can adopt two well-defined stacking orders: AA stacking, characterized by perfect atomic registry between adjacent layers, and AB stacking, characterized by a lateral shift of approximately half a unit cell. These configurations correspond to distinct local energy minima in the crystal lattice.[4] These stacking configurations exert strong influence on the material's vibrational, optical, and electronic responses. As such, stacking order constitutes an additional and independent structural degree of freedom for tuning the properties of ReS_2, beyond layer number and in-plane orientation.[5–7]

Similar to other vdW materials, ReS_2 exhibits strongly anisotropic thermal transport, with in-plane thermal conductivity ($\sim$70 W m^{-1} K^{-1} along Re-chain and $\sim$50 W m^{-1} K^{-1} perpendicular to Re-chain) substantially exceeding its cross-plane counterpart ($\sim$0.55 W m^{-1} K^{-1} in nanofilms), as reported by prior time-domain thermoreflectance (TDTR) measurements.[8] In vdW-based electronic and optoelectronic devices, heat generated in the active layers dissipates predominantly along the cross-plane direction through stacked layers and interfaces, making cross-plane thermal conductivity (κ_c) a critical bottleneck for device performance and reliability.[9] Understanding how interlayer registry controls cross-plane phonon transport is therefore essential for engineering next-generation vdW electronics and optoelectronics. Historically, cross-plane thermal transport in layered vdW materials was assumed to be dominated by phonons with very short mean free paths (MFPs), typically on the order of only a few nanometers. This picture has been fundamentally revised by recent experimental and theoretical studies on benchmark systems such as graphite[10–12] and MoS_2,[13] which demonstrate that room-temperature cross-plane phonon MFPs can extend to hundreds

of nanometers. Such unexpectedly long-range transport has been attributed to a phonon filtering effect, in which weak interlayer vdW interactions suppress short-MFP phonons and confine heat flow to long-MFP modes.

ReS_2 presents a unique and largely unexplored opportunity to examine cross-plane phonon transport in exceptional depth. Because its AA and AB stacking sequences remain remarkably stable across varying thicknesses, ReS_2 serves as an ideal platform for investigating and ultimately engineering cross-plane heat transport in ultrathin vdW devices. While earlier TDTR measurements reported no clear thickness dependence for ReS_2 films between 60 and 450 nm, these studies did not distinguish between stacking orders and therefore effectively averaged over fundamentally different interlayer configurations.[8] Consequently, the role of interlayer registry in governing phonon filtering, phonon MFPs, and the crossover between distinct transport regimes remains a critical and practically important open question.

In this work, we perform systematic picosecond transient thermoreflectance (ps-TTR) measurements of high-quality ReS_2 samples with well-defined AA or AB stacking orders that persist over micrometer-scale thicknesses. These measurements are thus capable of capturing an order-of-magnitude variation in κ_c with increasing sample thickness, as well as pronounced differences between AA- and AB-stacked ReS_2. By integrating the ps-TTR measurements with molecular dynamics simulations based on a deep-neural-network (DNN) potential trained on *ab initio* data, we further compare the spectral phonon properties of AA- and AB-stacked ReS_2 for both ambient pressure and high-pressure conditions. Through this combined experimental-computational approach, we elucidate the unique phonon transport behavior of ReS_2 and demonstrate it as a model system in which stacking order, interlayer coupling, and phonon filtering can be deliberately manipulated to tune cross-plane heat conduction from diffusive to quasi-ballistic and fully ballistic regimes.

Throughout this work, atomic registry refers to the relative crystallographic alignment between adjacent ReS_2 layers and should not be confused with phase coherence of phonon wave packets. Unless explicitly stated otherwise, the term ballistic transport denotes heat conduction in the limit where phonons traverse the film without notable internal scattering, whereas quasi-ballistic transport refers to the intermediate regime where both ballistic propagation and intrinsic scattering contribute. Finally, phonon filtering describes the preferential transmission of selected phonon frequencies or polarizations by the interlayer van der Waals interface rather than coherent wave interference.

Figures 1(a) and 1(b) show the atomic configurations of the AA and AB stacking orders in ReS_2. The stacking order of ReS_2 samples can be easily identified by measuring the difference between two Raman peaks: Δ = mode III–mode I. For AA stacking, $\Delta \sim 13\ cm^{-1}$, and for AB stacking, $\Delta \sim 20\ cm^{-1}$. We employed a re-exfoliation approach to confirm that a single, well-defined stacking order can persist over thicknesses of several micrometers (Figs. S1 and S2). Cross-plane thermal conductivities were measured using a ps-TTR technique[14,15] and extracted using a one-dimensional heat conduction model, as detailed in the supplementary material. The thickness-dependent κ_c for both AA and AB stackings is presented in Fig. 1(c). In the ultrathin regime (below 100 nm), both stacking configurations exhibit similar values, which is consistent with prior measurements[8] and suggests that thermal transport in the thinnest flakes is primarily constrained by boundary scattering. However, as thickness increases, the thermal behaviors of the two registries diverge significantly. While both configurations show a pronounced increase in κ_c with thickness, AA-stacked samples exhibit a more rapid rise and reach a clear saturation plateau of approximately 4.0 W m^{-1} K^{-1}. In contrast, AB stacking exhibits a slower recovery of κ_c and fails to reach saturation even as thicknesses approach 1 μm, trending toward an extrapolated bulk limit of approximately 2.0 W m^{-1} K^{-1}. This distinct bifurcation demonstrates that stacking order serves as a primary determinant of intrinsic cross-plane transport, while the delayed saturation in both registries provides direct experimental evidence of exceptionally long cross-plane phonon MFPs that far exceed the predictions of conventional kinetic theory.

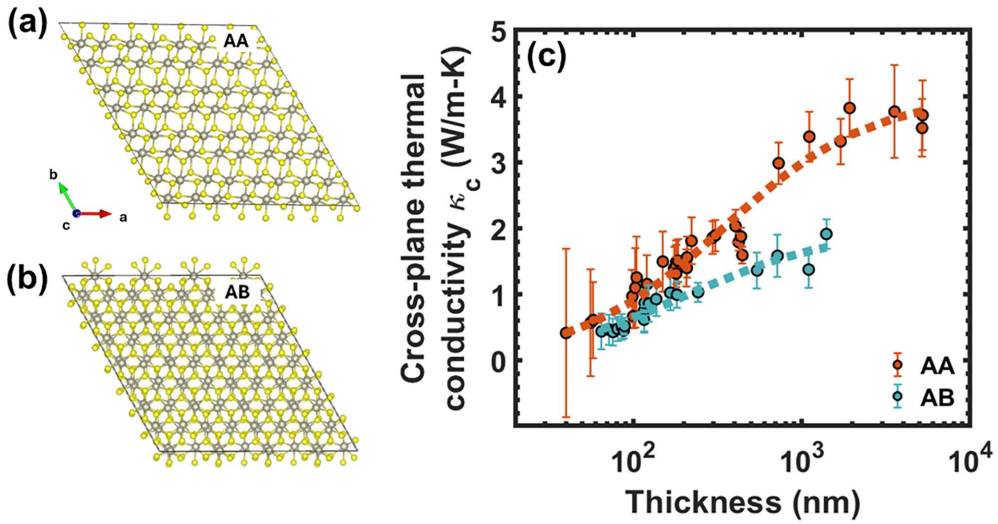

FIG. 1. (a) and (b) Atomic structures of AA- and AB-stacked ReS_2, where gray dots represent Re atoms and yellow dots represent S atoms. (c) Measured cross-plane thermal conductivity as a function of thickness for AA- and AB-stacked ReS_2. The dashed lines represent fittings with the gray phonon thermal transport model.[16,17]

To quantify the characteristic MFPs, we fit the experimental data for κ_c as a function of sample thickness d using the gray phonon thermal transport model,[16,17]

$$\kappa_c(d) = \kappa_{bulk}\frac{d}{d+\Lambda_{bulk}}.$$

The extracted bulk κ_c values are consistent with the measured saturation trends: ~4.0 W m^{-1} K^{-1} for AA stacking and ~2.0 W m^{-1} K^{-1} for AB stacking. The corresponding effective bulk-limit MFPs Λ_{bulk} are remarkably long, ~346 nm for AA and ~203 nm for AB. For comparison, a simple kinetic estimate, $\kappa_c \sim 1/3\, C v_c \Lambda_c$, using the total heat capacity C and cross-plane sound velocity v_c yields $\Lambda_c \approx 2.2$ nm for AA stacking, corresponding to only ~8 layers. The more than two-order-of-magnitude discrepancy is physically important: the total heat capacity is dominated by many modes that store thermal energy but do not efficiently carry cross-plane heat, whereas κ_c is dominated by a small subset of low-frequency acoustic modes with long wavelengths, high transmission, and long lifetimes. Thus, the apparent gray MFP extracted from thickness dependence should be interpreted as the transport-weighted length scale of heat-carrying phonons rather than the average MFP of all vibrational modes. Resolving these mode-dependent characteristics requires a detailed spectral analysis.

Figure 1 therefore establishes two critical experimental findings. First, κ_c is highly sensitive to stacking order, with AA stacking conducting heat nearly twice as efficiently as the AB configuration. Second, both registries exhibit exceptionally long phonon MFPs, confirming that cross-plane transport in ReS_2 is dominated by long-range modes rather than localized vibrations. These observations raise fundamental questions regarding why AA stacking supports much higher conductivity and what physical mechanism drives such long MFPs, which we address through mode-resolved spectral analysis in the following discussions.

To address why AA-stacking ReS_2 conducts heat more efficiently than its AB-stacking counterpart, we constructed a DNN interatomic potential, using the DeepMD approach,[18] from extensive *ab initio* molecular dynamics (AIMD) data for both stacking orders under different thermodynamic conditions. Details of the AIMD simulations and training of the DNN potential are presented in SI. Notably, the DNN potential shows an energy accuracy on the order of 10^{-4}–10^{-3} eV/atom, well agreeing with AIMD values. The accuracy of the DNN potential was further validated through non-equilibrium molecular dynamics (NEMD) simulations[19] performed at 300 K using LAMMPS.[20] As demonstrated in Fig. S5 of the supplementary material, the NEMD results reproduce the experimentally measured κ_c for both stacking orders up to ~300 nm, confirming that the DNN potential reliably captures the size-dependent thermal transport in both types of ReS_2.

Bulk-limit thermal conductivities were subsequently obtained using equilibrium molecular dynamics (EMD)[21] and the Green–Kubo formalism.[22,23] The predicted bulk κ_c values are approximately 4.5 W ± 0.12 m^{-1} K^{-1} for AA stacking and 3.2 ± 0.11 W m^{-1} K^{-1} for AB stacking. These values are higher than the experimental bulk limits, as expected for defect-free simulations (see Sec. 13 of the supplementary material for the effect of isotopes and point-defect on κ_c), but they reproduce the key physical trend: AA stacking supports substantially stronger cross-plane heat conduction than AB stacking. This agreement indicates that the stacking dependence is intrinsic and originates from changes in phonon dispersion and anharmonic scattering rather than from extrinsic sample-to-sample variations.

The observed stacking dependence is unlikely to originate from sample-to-sample variations. The AA and AB stacking orders were identified using an established Raman-based protocol that was previously validated by complementary polarized photoluminescence, ultrafast pump-probe spectroscopy, and first-principles calculations across multiple independent ReS_2 crystals.[4] Furthermore, the DNN-MD simulations performed on defect-free structures reproduce the same ordering of thermal conductivity ($\kappa_{AA} > \kappa_{AB}$), as shown in Fig. S5 of the supplementary material, providing independent evidence that the difference arises from the intrinsic phonon transport characteristics associated with stacking order rather than extrinsic sample variability.

Spectral energy density (SED) analysis[24] was used to extract phonon dispersions, group velocities, lifetimes, and MFPs. Figure 2(a) shows that the longitudinal acoustic (LA) branch in AA-stacking ReS_2 has a slightly steeper cross-plane dispersion than that in AB-stacking ReS_2, while the two transverse acoustic (TA) branches remain nearly degenerate in AA stacking but split clearly in AB stacking, consistent

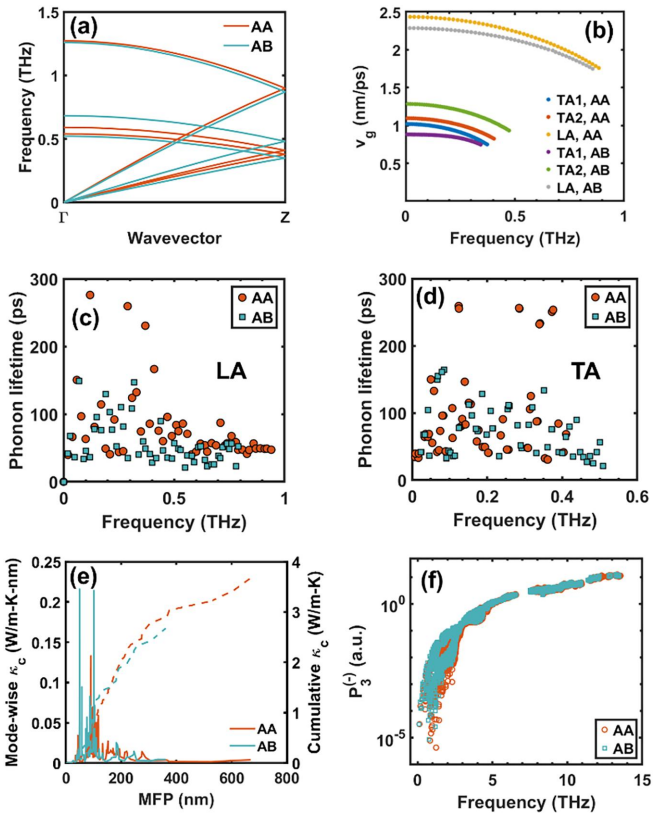

FIG. 2. Mode-resolved phonon properties of AA- and AB-stacked ReS_2 from SED calculations. (a) Phonon dispersion relations for AA- and AB-stacked ReS_2. (b) Mode-resolved phonon group velocities. (c,d) Phonon lifetimes for AA and AB stacking extracted from Lorentzian fitting of SED spectra. (e) Left axis: mode-wise cross-plane thermal conductivity. Right axis: cumulative cross-plane thermal conductivity. (f) The emission process of three-phonon scattering phase space for AA- and AB-stacked ReS_2.

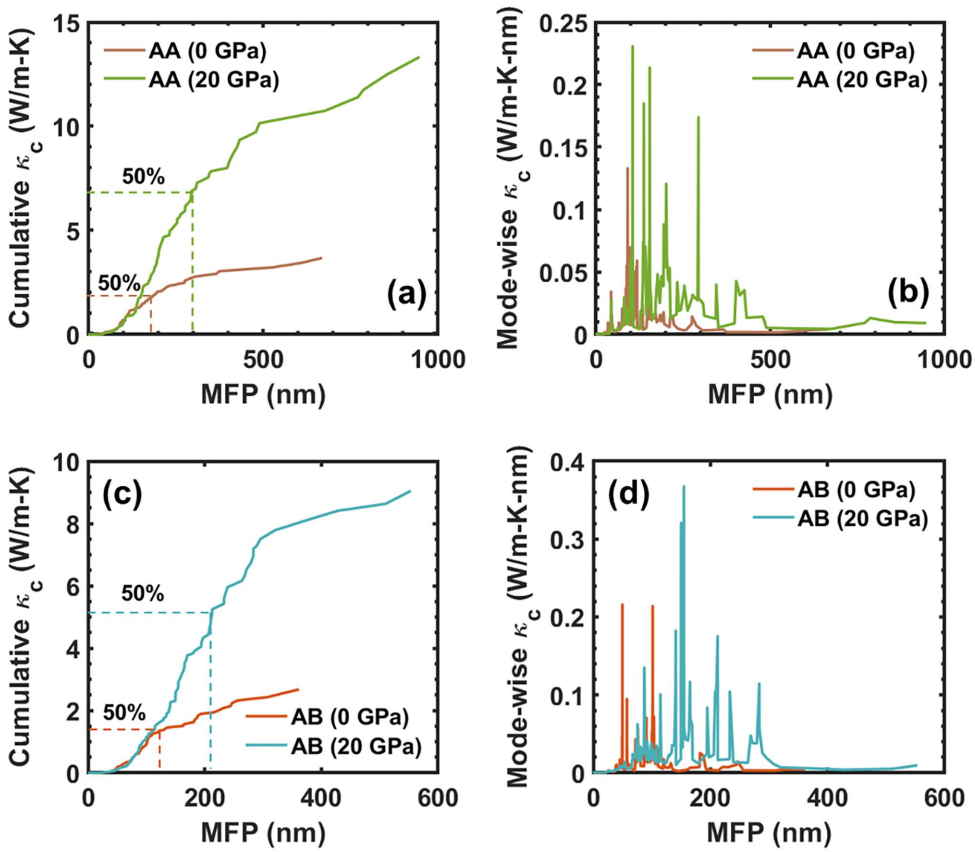

FIG. 3. *Cumulative cross-plane thermal conductivity as a function of phonon MFP for AA- and AB-stacked ReS_2 under different pressures.* (a) and (c) Cumulative cross-plane thermal conductivity vs MFP at 0 and 20 GPa for AA- and AB-stacked ReS_2, respectively. (b) and (d) Corresponding mode-wise cross-plane thermal conductivity spectra displaying the distribution of phonon contributions across MFPs.

with our density functional theory (DFT) calculations (Fig. S8 in the supplementary material). The corresponding group velocities [Fig. 2(b)] alone cannot explain the substantially higher bulk κ_c of AA stacking: AA stacking has modestly higher phonon group velocities for the LA branch, whereas AB shows somewhat higher phonon group velocities for the TA branches. The decisive difference instead lies in the phonon lifetimes.

Figures 2(c) and 2(d) show that both LA and TA phonons in AA-stacked ReS_2 have systematically longer lifetimes than their counterparts in AB-stacked ReS_2, providing the microscopic origin of the higher κ_c in AA stacking. As shown in Figs. 2(a) and 2(b), the two TA branches remain nearly degenerate in AA stacking, restricting the number of three-phonon processes that can simultaneously satisfy energy and momentum conservation. In contrast, the lateral registry shift in AB stacking lifts this degeneracy and produces two distinct TA branches. The resulting branch splitting increases the number of allowed scattering channels, particularly emission processes in which one higher-frequency acoustic phonon decays into two lower-frequency modes. Consistent with this interpretation, Fig. 2(f) shows a larger three-phonon emission phase space for AB-stacked ReS_2 than for its AA-stacked counterpart. Consequently, the cumulative κ_c spectrum in Fig. 2(e) contains a stronger long-MFP contribution for AA-stacked ReS_2. Phase space alone does not determine the scattering rate, which also depends on anharmonic interaction strengths; nonetheless, it provides mechanistic support for the shorter lifetimes obtained directly from the SED analysis. These results show that the atomic registry of different stackings has a concrete phonon-physics meaning in this system: vertical layer alignment preserves acoustic-branch degeneracy and reduces anharmonic phase space, whereas the shifted AB registry breaks this degeneracy and accelerates phonon relaxation.

We next examine why ReS_2 supports such long cross-plane MFPs. Similar thickness-dependent measurements on graphite and MoS_2 consistently indicate that long-MFP phonons dominate cross-plane heat conduction. In graphite, the c-axis phonon MFP has been estimated to be ~200 nm,[10,11] while in MoS_2, phonons with MFPs exceeding ~200 nm contribute more than 50% of the total κ_c.[12] These unexpectedly long MFPs have been attributed to the so-called phonon filtering effect, in which the weak interlayer vdW forces suppress short-MFP phonons and preferentially allow long-MFP modes to transmit across layers. If this conventional understanding of phonon filtering effect holds, one would expect the filtering effect to depend strongly on interlayer bonding strength: weaker vdW force → stronger filtering → a larger contribution from longer-MFP phonons (i.e.,

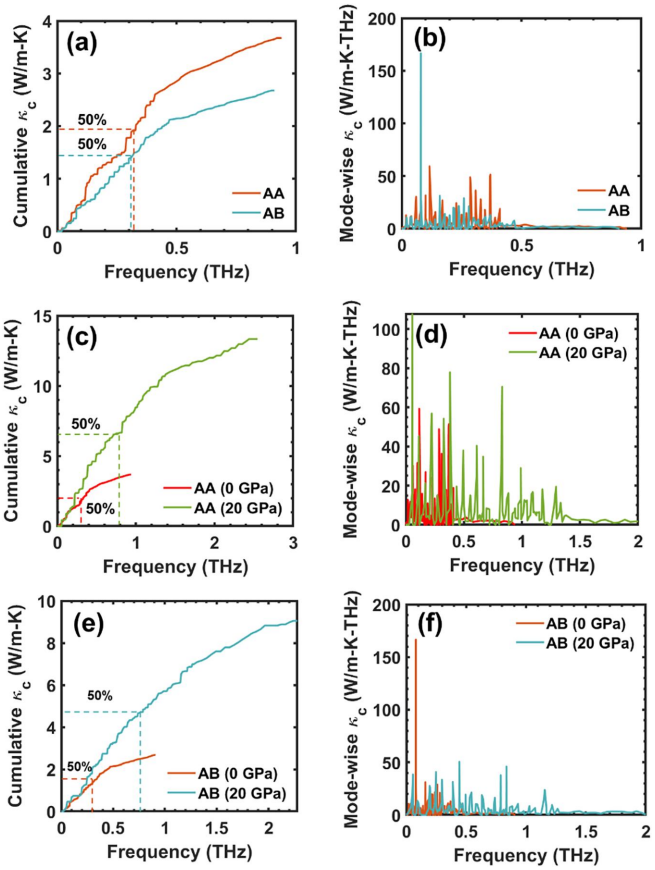

FIG. 4. *Cumulative cross-plane thermal conductivity as a function of phonon frequency for AA- and AB-stacked ReS_2 under different pressures.* (a), (c), and (e) Cumulative cross-plane thermal conductivity vs frequency at 0 and 20 GPa for AA- and AB-stacked ReS_2, respectively. (b), (d), and (f) Corresponding mode-wise cross-plane thermal conductivity spectra displaying the distribution of phonon contributions in the frequency domain.

a spectral shift of mode-wise κ_c toward longer MFP), and conversely, stronger interlayer coupling should weaken filtering, and contribution from short-MFP phonons should increase (i.e., a spectral shift of mode-wise κ_c toward shorter MFP).

Hydrostatic pressure provides a convenient means of tuning the interlayer coupling in vdW materials and tests this conventional picture of phonon filtering effect. While high-pressure experiments are beyond the scope of this work, we performed SED analysis using our DNN potential to investigate the effects of pressure. Hydrostatic pressure was applied using a Nosé–Hoover barostat[25,26] in all three directions. We calculated the cumulative κ_c as a function of MFP for both AA and AB stackings at 0 and 20 GPa, respectively. As shown in Figs. 3(a) and 3(c), higher pressure (i.e., stronger interlayer coupling) shifts the cumulative κ_c curves toward longer MFPs for both stackings. For AA stacking, phonons with $\Lambda < 180$ nm contribute 50% of κ_c at 0 GPa, but the 50% cutoff increases to ~300 nm at 20 GPa. For AB stacking, the cutoff shifts from ~120 nm at 0 GPa to above 200 nm at 20 GPa. The corresponding mode-wise κ_c spectra [Figs. 3(b) and 3(d)] further confirm that stronger interlayer interaction at higher pressure extends the phonon contribution into the long-MFP regime. This trend arises because applying pressure increases the group velocity $v_c(\omega)$, while phonon lifetimes $\tau(\omega)$ change only weakly (as shown in Fig. S9); as a result, the MFP $\Lambda_c(\omega)=v_c(\omega)\tau(\omega)$ becomes longer even though the spectral filter becomes less selective. These observations seem to contradict the conventional understanding of phonon filtering and indicate that the relationship between phonon filtering and MFP requires careful reexamination.

Because phonon filtering is fundamentally a frequency-domain process, we analyzed cumulative κ_c as a function of phonon frequency in Fig. 4. At 0 GPa, both AA and AB stackings show that ~50% of the κ_c arises from phonons around 0.3 THz [Fig. 4(a)], and virtually all contributing modes lie below ~0.5 THz [Fig. 4(b)]. When pressure increases to 20 GPa, however, the transmission bandwidth broadens dramatically, extending to ~1.5 THz [Figs. 4(d) and 4(f)], and the cumulative κ_c curves gain substantial weight at higher frequencies [Figs. 4(c) and 4(e)]. This indicates that weak vdW interactions at low pressure act as a strong low-pass *spectral* filter, effectively blocking high-frequency modes and transmitting primarily low-frequency, long-wavelength phonons.

We quantify the filtering strength using a cutoff frequency $\omega_{cut} = 0.5$ THz and the filtering fraction $F(\omega_{cut}) = \kappa(\omega < \omega_{cut})/\kappa_{max}$. For AA stacking, F decreases from 78.4% at 0 GPa to 37.22% at 20 GPa; for AB stacking, it decreases from 80.0% to 35.97%. The nearly identical values for AA and AB indicate that filtering strength is governed primarily by the interlayer coupling strength, while the difference between AA and AB conductivities arises mainly from stacking-dependent lifetimes and scattering phase space. This separation of roles is important: interlayer force determines which frequencies can transmit across the vdW gap, whereas stacking registry determines how long those transmitted acoustic phonons survive.

These results clarify the physical meaning of phonon filtering in vdW materials. Phonon filtering should be defined as the preferential transmission of low-frequency, long-wavelength modes across weak interlayer bonds. Because this mechanism originates from the wave nature of phonons,[27] it is most naturally described in the frequency domain and is closely analogous to optical low-pass filtering.[28] This definition resolves the ambiguity in the literature,[29,30] where the thermal consequences of filtering are often expressed in the MFP domain, since Λ determines how far each transmitted mode carries heat. Our results show that these two perspectives must be considered together: phonon filtering is fundamentally a spectral effect, and weaker interlayer coupling narrows the phonon bandwidth (stronger filtering at 0 GPa, Fig. 4), whereas the MFP spectrum reflects the transport outcome of the modes that pass through that filter, resulting in shorter Λ at 0 GPa due to lower phonon group velocities (Fig. 3).

To further elucidate the thickness dependence of cross-plane heat transport, the measured κ_c was converted to thermal resistance using $R = t/\kappa_c$, where t is the film thickness. As shown in Fig. 5(a), the resistance of ReS_2 does not scale linearly with film thickness; instead, it exhibits a sublinear saturating trend as the thickness decreases, a hallmark of quasi-ballistic transport,[13,31] in which phonon MFPs are comparable to the film thickness. In the thinnest flakes (<150 nm), both AA- and AB-stacked samples display a clear plateau in resistance, indicating that the heat flow has transitioned into the fully ballistic regime where the conductance becomes thickness-independent.[32,33] This behavior is faithfully reproduced by our NEMD simulations. From the

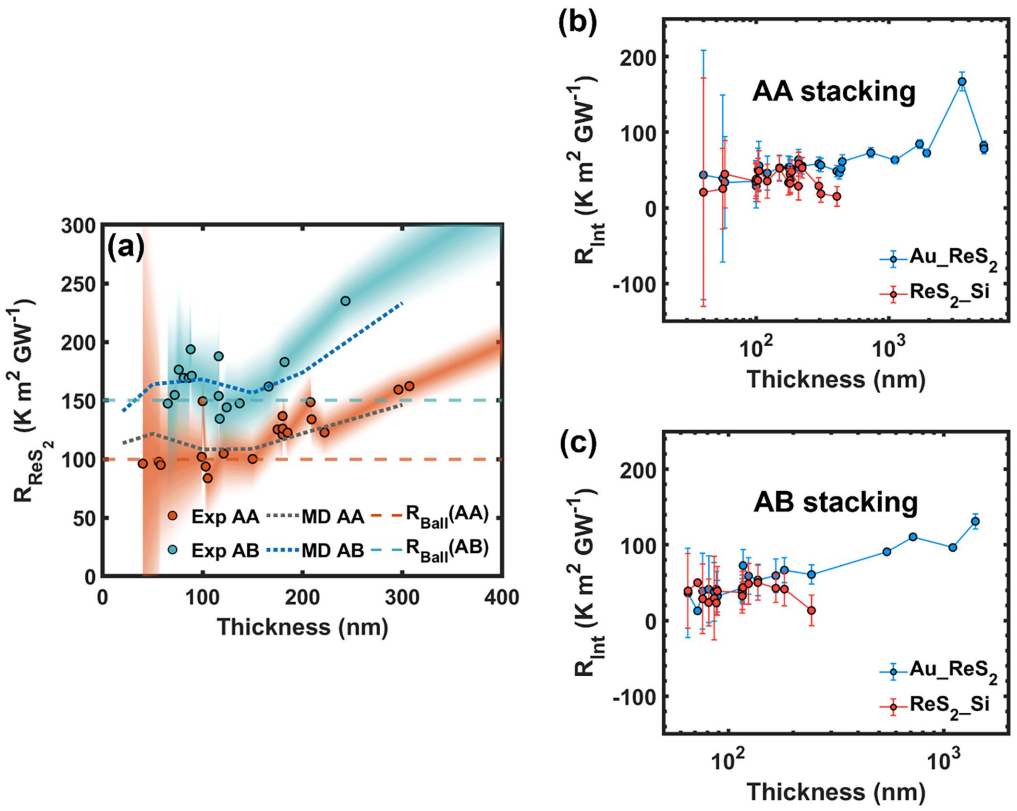

FIG. 5. (a) Thickness-dependent cross-plane thermal resistance of AA- and AB-stacked ReS_2, with corresponding NEMD simulation results, where the shaded regions represent the error bars. (b) Thickness-dependent contact resistances at the Au/ReS_2 and ReS_2/Si interfaces for AA-stacked samples. (c) Thickness-dependent contact resistances at the Au/ReS_2 and ReS_2/Si interfaces for AB-stacked samples.

magnitude of the plateau, we extract ballistic thermal resistances of $R_{ball} \approx 150\ m^2\,K\,GW^{-1}$ for AB stacking and $\approx 100\ m^2\,K\,GW^{-1}$ for AA stacking, values an order of magnitude larger than those reported for MoS_2 ($\sim 10\ m^2\,K\,GW^{-1}$).[13] Figures 5(b) and 5(c) present the corresponding thickness-dependent contact resistances for both stacking orders. The contact resistances show no systematic dependence on thickness, and the values at the Au/ReS_2 interface ($\sim 50\ m^2\,K\,GW^{-1}$ or $20\ MW\ m^{-1}\,K^{-1}$) agree well with previously reported TDTR measurements and further confirm that the thickness-dependent trends do come from intrinsic thermal transport in ReS_2.[8]

The direct experimental observation of the ballistic limit in ReS_2 is a notable outcome of this study, enabled by two key factors. First, the ps-TTR technique, with its single-pulse excitation and long delay-time window, captures the intrinsic thermal response of ultrathin films without cumulative heating, allowing early-time ballistic transport to be resolved. Second, the exceptionally long and stacking-dependent cross-plane phonon MFPs in ReS_2, arising from its weak and registry-sensitive vdW coupling, ensure that the condition $t \lesssim \Lambda_c$ is reached at experimentally accessible thicknesses, permitting the ballistic resistance plateau to emerge directly in the measurements. The resulting finite plateau value, R_{ball}, represents the intrinsic ballistic resistance, reflecting the fundamental phonon transmission across atomic layers and setting the upper bound for heat dissipation in ultrathin ReS_2. The substantially larger R_{ball} in ReS_2 compared with MoS_2 indicates a much lower intrinsic phonon transparency across its vdW gaps, consistent with a narrower spectral window that admits only low-frequency, long-wavelength phonons. The contrast between AA and AB stacking demonstrates that stacking order can serve as a practical tuning parameter for R_{ball}, enabling control over interlayer phonon transmission by modifying registry and coupling strength. Such tunability offers a new approach to engineering vdW thermal filters, phononic interfaces, and low-conductance barriers for 2D electronics and optoelectronic devices.[10–13,34]

In summary, this work demonstrates that stacking order, an aspect largely neglected in prior studies of vdW materials, is a key determinant of cross-plane phonon thermal transport in ReS_2, with implications for thermal transport engineering in ReS_2 and other vdW materials. By integrating systematic ps-TTR measurements on micrometer-scale crystals with single stacking order, and deep-learning-based molecular dynamics simulations and SED analysis, we demonstrate that both AA and AB stacking orders support exceptionally long phonon MFP and exhibit distinct transitions from quasi-ballistic to fully ballistic transport as the sample thickness decreases below ~ 150 nm. Notably, AA-stacking ReS_2 exhibits significantly higher κ_c than its AB-stacking counterpart, which is attributed to longer acoustic phonon lifetimes enabled by the perfect atomic registry

of AA stacking. Furthermore, pressure-dependent analyses reveal that phonon filtering in ReS_2 is a fundamentally frequency-selective mechanism, in which weak vdW coupling produces a low-pass filtering effect that is highly tunable through interlayer coupling. We further show that weak interlayer coupling at ambient pressure preferentially transmits low-frequency, long-wavelength phonons whose MFPs extend over hundreds of nanometers, whereas stronger coupling at high pressure increases the MFP primarily by enhancing phonon group velocities. By connecting the frequency-domain filtering picture with the resulting MFP distributions, ReS_2 provides a useful platform for the spectral engineering of thermal transport in diverse vdW materials.

Additional details on the experimental validation, computational methods, and supporting analyses are provided in the supplementary material. These include verification of the stacking order through re-exfoliation and Raman characterization, development and validation of the deep neural network interatomic potential, molecular dynamics simulation details, phonon properties and scattering analysis, pressure-dependent lattice dynamics calculations, uncertainty and sensitivity analyses of the thermal measurements, and the effects of isotope disorder and point defects on cross-plane thermal transport.

See the supplementary material for additional details on stacking verification, computational and experimental methods, phonon transport analyses, and uncertainty and defect effects in ReS_2.

Yongjian Zhou, Zefang Ye, and Yaguo Wang acknowledge the funding support from the National Science Foundation (NSF-CBET Award No. 2211660). Haoran Cui and Yan Wang acknowledge the support from the National Science Foundation (NSF-CBET Award No. 2211696).

AUTHOR DECLARATIONS

Conflict of Interest

The authors have no conflicts to disclose.

Author Contributions

Yongjian Zhou, Haoran Cui, and Zefang Ye contributed equally to this paper.

Yongjian Zhou: Data curation (equal); Formal analysis (equal); Investigation (equal); Methodology (equal); Software (equal); Validation (equal); Writing – original draft (equal); Writing – review & editing (equal). **Haoran Cui:** Data curation (equal); Formal analysis (equal); Investigation (equal); Methodology (equal); Software (equal); Validation (equal); Writing – original draft (equal); Writing – review & editing (equal). **Zefang Ye:** Data curation (equal); Formal analysis (equal); Investigation (equal); Methodology (equal); Software (equal); Validation (equal); Writing – original draft (equal); Writing – review & editing (equal). **Jung-Fu Lin:** Conceptualization (equal); Methodology (equal); Validation (equal); Writing – review & editing (equal). **Yan Wang:** Conceptualization (equal); Funding acquisition (equal); Investigation (equal); Methodology (equal); Project administration (equal); Resources (equal); Supervision (equal); Writing – original draft (equal); Writing – review & editing (equal). **Yaguo Wang:** Conceptualization (equal); Formal analysis (equal); Funding acquisition (equal); Investigation (equal); Methodology (equal); Project administration (equal); Resources (equal); Supervision (equal); Validation (equal); Writing – original draft (equal); Writing – review & editing (equal).

DATA AVAILABILITY

The data that support the findings of this study are available from the corresponding authors upon reasonable request.

REFERENCES

[1]J. Shim, A. Oh, D. Kang, S. Oh, S. K. Jang, J. Jeon, M. H. Jeon *et al.*, "High-performance 2D rhenium disulfide (ReS_2) transistors and photodetectors by oxygen plasma treatment," Adv. Mater. **28**(32), 6985–6992 (2016).
[2]X. Su, B. Zhang, Y. Wang, G. He, G. Li, N. Lin, K. Yang, J. He, and S. Liu, "Broadband rhenium disulfide optical modulator for solid-state lasers," Photonics Res. **6**(6), 498–505 (2018).
[3]X. Meng, Y. Zhou, K. Chen, R. H. Roberts, W. Wu, J. Lin, R. T. Chen, X. Xu, and Y. Wang, "Anisotropic saturable and excited-state absorption in bulk ReS_2," Adv. Opt. Mater. **6**(14), 1800137 (2018).
[4]Y. Zhou, N. Maity, A. Rai, R. Juneja, X. Meng, A. Roy, Y. Zhang *et al.*, "Stacking-order-driven optical properties and carrier dynamics in ReS_2," Adv. Mater. **32**(22), 1908311 (2020).
[5]Y. Zhou, N. Maity, J.-F. Lin, A. K. Singh, and Y. Wang, "Nonlinear optical absorption of ReS_2 driven by stacking order," ACS Photonics **8**(2), 405–411 (2021).
[6]Y. Zhou and Y. Wang, "Wavelength and stacking order dependent exciton dynamics in bulk ReS_2," Adv. Opt. Mater. **10**(23), 2201322 (2022).
[7]Y. Chen, J. Lin, J. Jiang, D. Wang, Y. Yu, S. Li, J. Pan *et al.*, "Constructing slip stacking diversity in van der Waals homobilayers," Adv. Mater. **36**(36), 2404734 (2024).
[8]H. Jang, C. R. Ryder, J. D. Wood, M. C. Hersam, and D. G. Cahill, "3D anisotropic thermal conductivity of exfoliated rhenium disulfide," Adv. Mater. **29**(35), 1700650 (2017).
[9]L. Zhang, Y. Zhong, X. Qian, Q. Song, J. Zhou, L. Li, L. Guo, G. Chen, and E. N. Wang, "Toward optimal heat transfer of 2D–3D heterostructures via van der Waals binding effects," ACS Appl. Mater. Interfaces **13**(38), 46055–46064 (2021).
[10]H. Zhang, X. Chen, Y.-D. Jho, and A. J. Minnich, "Temperature-dependent mean free path spectra of thermal phonons along the c-axis of graphite," Nano Lett. **16**(3), 1643–1649 (2016).
[11]Z. Wei, J. Yang, W. Chen, K. Bi, D. Li, and Y. Chen, "Phonon mean free path of graphite along the c-axis," Appl. Phys. Lett. **104**(8), 081903 (2014).
[12]J. Crosby, H. Cui, and Y. Wang, "Significant ballistic thermal transport across graphene layers: Effect of nanoholes and lithium intercalation," Appl. Phys. Lett. **127**(8), 082201 (2025).
[13]A. Sood, F. Xiong, S. Chen, R. Cheaito, F. Lian, M. Asheghi, Y. Cui, D. Donadio, K. E. Goodson, and E. Pop, "Quasi-ballistic thermal transport across MoS_2 thin films," Nano Lett. **19**(4), 2434–2442 (2019).
[14]J. Jeong, X. Meng, A. K. Rockwell, S. R. Bank, W.-P. Hsieh, J.-F. Lin, and Y. Wang, "Picosecond transient thermoreflectance for thermal conductivity characterization," Nanoscale Microscale Thermophys. Eng. **23**(3), 211–221 (2019).
[15]Z. Ye, J. Park, Y. Zhang, X. Meng, M. Disiena, S. K. Banerjee, J.-F. Lin, and Y. Wang, "Simultaneous determination of thermal conductivity and heat capacity in thin films with picosecond transient thermoreflectance and picosecond laser flash," Nanoscale Microscale Thermophys. Eng. **27**(3–4), 182–194 (2023).
[16]A. S. M. E. Majumdar, "Microscale heat conduction in dielectric thin films," J. Heat Transfer **115**(1) 7–16 (1993).
[17]J. Kaiser, T. Feng, J. Maassen, X. Wang, X. Ruan, and M. Lundstrom, "Thermal transport at the nanoscale: A Fourier's law vs. phonon Boltzmann equation study," J. Appl. Phys. **121**(4), 044302 (2017).
[18]H. Wang, L. Zhang, J. Han, and W. E, "DeePMD-kit: A deep learning package for many-body potential energy representation and molecular dynamics," Comput. Phys. Commun. **228**, 178–184 (2018).
[19]T. Ikeshoji and B. Hafskjold, "Non-equilibrium molecular dynamics calculation of heat conduction in liquid and through liquid-gas interface," Mol. Phys. **81**(2), 251–261 (1994).

[20]A. P. Thompson, H. M. Aktulga, R. Berger, D. S. Bolintineanu, W. M. Brown, P. S. Crozier, P. J. In't Veld *et al.*, "LAMMPS-a flexible simulation tool for particle-based materials modeling at the atomic, meso, and continuum scales," Comput. Phys. Commun. **271**, 108171 (2022).
[21]A. J. H. McGaughey and J. M. Larkin, "Predicting phonon properties from equilibrium molecular dynamics simulations," Annu. Rev. Heat Transfer **17**, 49 (2014).
[22]S. G. Volz and G. Chen, "Molecular-dynamics simulation of thermal conductivity of silicon crystals," Phys. Rev. B **61**(4), 2651 (2000).
[23]H. Cui, T. Maranets, T. Ma, and Y. Wang, "Spectral analysis of coherent and incoherent phonon transport in silicon nanomeshes," Phys. Rev. B **110**(7), 075301 (2024).
[24]J. A. Thomas, J. E. Turney, R. M. Iutzi, C. H. Amon, and A. J. H. McGaughey, "Predicting phonon dispersion relations and lifetimes from the spectral energy density," Phys. Rev. B **81**(8), 081411 (2010).
[25]S. Nosé, "A unified formulation of the constant temperature molecular dynamics methods," J. Chem. Phys. **81**(1), 511–519 (1984).
[26]W. G. Hoover, "Canonical dynamics: Equilibrium phase-space distributions," Phys. Rev. A **31**(3), 1695 (1985).
[27]C. Kittel and P. McEuen, *Introduction to Solid State Physics* (John Wiley & Sons, 2018).
[28]M. Born and E. Wolf, *Principles of Optics: Electromagnetic Theory of Propagation, Interference and Diffraction of Light* (Elsevier, 2013).
[29]M. N. Luckyanova, J. Garg, K. Esfarjani, A. Jandl, M. T. Bulsara, A. J. Schmidt, A. J. Minnich *et al.*, "Coherent phonon heat conduction in superlattices," Science **338**(6109), 936–939 (2012).
[30]L. Zeng, K. C. Collins, Y. Hu, M. N. Luckyanova, A. A. Maznev, S. Huberman, V. Chiloyan *et al.*, "Measuring phonon mean free path distributions by probing quasiballistic phonon transport in grating nanostructures," Sci. Rep. **5**(1), 17131 (2015).
[31]R. Anufriev, S. Gluchko, S. Volz, and M. Nomura, "Quasi-ballistic heat conduction due to Lévy phonon flights in silicon nanowires," ACS Nano **12**(12), 11928–11935 (2018).
[32]J. Lee, J. Lim, and P. Yang, "Ballistic phonon transport in holey silicon," Nano Lett. **15**(5), 3273–3279 (2015).
[33]D. Vakulov, S. Gireesan, M. Y. Swinkels, R. Chavez, T. Vogelaar, P. Torres, A. Campo *et al.*, "Ballistic phonons in ultrathin nanowires," Nano Lett. **20**(4), 2703–2709 (2020).
[34]H. Cui, I. R. Panneerselvam, P. Chakraborty, Q. Nian, Y. Liao, and Y. Wang, "Significantly enhanced interfacial thermal transport between single-layer graphene and water through basal-plane oxidation," Carbon **234**, 119910 (2025).